Uncertainty quantification in computational linear structural dynamics for viscoelastic composite structures

Rémi Capillon, Christophe Desceliers, Christian Soize

Uncertainty quantification in computational linear structural dynamics for viscoelastic composite structures

R. Capillon, C. Desceliers, C. Soize[1]

Université Paris-Est, Laboratoire Modélisation et Simulation Multi-Echelle, MSME UMR 8208 CNRS, 5 bd Descartes, 77454 Marne-la-Vallée, France

Abstract

This paper deals with the analysis of a stochastic reduced-order computational model in computational linear dynamics for linear viscoelastic composite structures in the presence of uncertainties. The computational framework proposed is based on a recent theoretical work that allows for constructing the stochastic reduced-order model using the nonparametric probabilistic approach. In the frequency domain, the generalized damping matrix and the generalized stiffness matrix of the stochastic computational reduced-order model are random matrices. Due to the causality of the dynamical system, these two frequency-dependent random matrices are statistically dependent and are linked by a compatibility equation induced by the causality of the system, involving a Hilbert transform. The computational aspects related to the nonparametric stochastic modeling of the reduced stiffness matrix and the reduced damping matrix that are frequency-dependent random matrices are presented. A dedicated numerical approach is developed for obtaining an efficient computation of the Cauchy principal value integrals involved in those equations for which an integration over a broad frequency domain is required. A computational analysis of the propagation of uncertainties is conducted for a composite viscoelastic structure in the frequency range. It is shown that the uncertainties on the damping matrix have a strong influence on the observed statistical dispersion of the stiffness matrix.

Keywords: Uncertainty quantification, Viscoelastic, Nonparametric probabilistic approach, Structural dynamics, Hilbert transform, Kramers-Kronig relations, Reduced-order model

[1]Corresponding author, christian.soize@univ-paris-est.fr

1. Introduction

In structural engineering, it is nowadays recognized that uncertainties coming from various sources have to be accounted for during the design and the analysis of a structure using computational models. In the computational models, the sources of uncertainties are due to the model-parameters uncertainties (for instance, the mechanical properties of the materials), as well as the model uncertainties induced by modeling errors (for instance due to the use of kinematic reductions such as the use of beams, plates, and shells, the lack of knowledge concerning the boundary conditions, etc). In addition, the computational models must have the capability to produce robust predictions that take into account the variability induced by the manufacturing process. In the probabilistic framework, uncertainty quantification has extensively be developed in the last two decades (see for instance [1, 2, 3, 4, 5] and references included).

The objective of this paper is to present the numerical analysis, the computational aspects, and the validation of an extension (recently proposed in [6, 7]) of the nonparametric probabilistic approach of uncertainties [2, 5, 8] in computational linear structural dynamics for viscoelastic composite structures. The proposed methodology, which is devoted to the development of a nonparametric probabilistic tool for the stochastic modeling of the uncertainties in computational viscoelastic models, is a strict extension of the previous works, in particular those devoted to experimental validations (see for instance [9, 10, 11, 12, 13, 14, 15, 16, 17, 18, 19, 20, 21] and references included).

The present work is devoted to the frequency-domain analysis of uncertain viscoelastic structures using the nonparametric probabilistic approach of uncertainty. The approach is formulated for a 3D dissipative composite structure made up of a linear viscoelastic part coupled with an elastic part. In the framework of linear viscoelasticity (see for instance [22, 23, 24]) and in the frequency domain, the generalized damping matrix $[\mathcal{D}(\omega)]$ and the generalized stiffness matrix $[\mathcal{K}(\omega)]$ of the reduced-order computational model depend on frequency ω. The nonparametric probabilistic approach of uncertainties consists in modeling this two frequency-dependent generalized matrices by frequency-dependent random matrices $[\mathbf{D}(\omega)]$ and $[\mathbf{K}(\omega)]$ respectively. However, as these two matrices come from a causal dynamical system, the causality implies two compatibility equations, also known as the Kramers-Kronig relations [25, 26], involving the Hilbert transform [27]. Consequently, the stochastic modeling of random matrices $[\mathbf{D}(\omega)]$ and $[\mathbf{K}(\omega)]$ cannot be constructed as independent random matrices without violating the causality as explained in [6].

The development of the stochastic model is performed in the framework of the general theory of the linear viscoelasticity of 3D-continuum media [22]. In this theory, there are no computational restrictions. The proposed stochastic model is thus consistent with the general theory and consequently, has also no restriction for its use. Concerning the construction of the nominal com-

putational model, it is assumed that any approximation of the general linear viscoelastic theory, which would be introduced for any reason, stays consistent with the general theory of linear viscoelasticity.

It should be noted that the Kramers-Kronig relations are automatically satisfied for the frequency-dependent damping and stiffness matrices of the nominal computational model related to any linear viscoelastic structure for which the constitutive equations of its viscoelastic parts are chosen in the class of causal models such as the generalized Maxwell model. However, the objective of this paper does not consist in revisiting the numerous papers and books related to the damping models for the damped structures that are not relevant of the linear viscoelasticity or the viscoelastic models used for constructing the nominal computational model of a linear viscoelastic structure. The paper concerns the frequency-dependent generalized damping and stiffness random matrices that are constructed by using the nonparametric probabilistic approach of uncertainties, for which the Kramers-Kronig relations are not satisfied as explained before. In this paper, the Kramers-Kronig relations do not need to be evoked for the nominal computational model under consideration for which the causality is assumed to be satisfied. Consequently, even if the the nominal linear viscoelastic structure is constructed with causal constitutive equations, it is necessary to constrain the stochastic construction with Kramers-Kronig relations [6, 7].

In this paper, a Monte Carlo stochastic solver (see for instance [28, 29]) is used to compute the random response of the system as well as statistical quantities, like confidence regions for instance. The compatibility equations are then used directly in order to generate compatible realizations of $[\mathbf{K}(\omega)]$ and $[\mathbf{D}(\omega)]$. As these equations have to be solved for a large number of values of the frequency, an efficient numerical algorithm has been developed and has been implemented in a finite element code in order to reduce the computational cost. Indeed, as the Hilbert transform is involved, it is necessary to compute an integral of the frequency-dependent matrices over the infinite frequency domain, for an integral that is defined in the Cauchy principal value sense. The proposed algorithm consists in a mixed integration technique in order to treat the singularity as well as integrating over an infinite interval, making use of an interpolation technique for positive-definite matrices and of orthogonal polynomials approximations (see [30, 31, 32, 33, 34]). In order to analyze the influence of viscoelasticity and causality in the propagation of uncertainties, a composite structure is studied in the Low-Frequency (LF) range. This structure is a multi-layer composite plate made up of two different viscoelastic layers and of a central elastic part. For such a structure, the memory effect induced by the viscoelasticity is clearly observed. The study of the behavior of the constructed stochastic model shows a strong influence of the level of uncertainties on $[\mathbf{D}(\omega)]$ in the statistical dispersion of $[\mathbf{K}(\omega)]$. The statistical fluctuations increase as a function of frequency because the uncertainties propagate from $[\mathbf{D}(\omega)]$ to $[\mathbf{K}(\omega)]$ through the Kramers-Kronig relations. It appears that a stochastic model, which satisfies the causality property, is necessary in

order to correctly quantify uncertainties in the dissipative structures.

A summary of the construction of the deterministic reduced-order computational model is presented in Section 2. Section 3 deals with the construction of the nonparametric probabilistic model using the Hilbert transform. Section 4 is devoted to the computational aspects of the proposed methodology used to circumvent the computational difficulties involved in calculating the Hilbert transform and in the analysis of the uncertainty propagation. In Section 5 a numerical example is presented.

Remarks about the notations. In this paper, the Fourier transform with respect to time t of any function f is denoted by $\widehat{f}$ such that $\widehat{f}(\omega) = \int_{\mathbb{R}} e^{-\mathrm{i}\,\omega t} f(t) dt$.

2. Summarizing the deterministic reduced-order computational model

This section is a summary devoted to the construction of the deterministic reduced-order computational dynamical model for a viscoelastic structure for which the notations, the developments, and the mathematical properties presented are taken from [7] and [24]. Such a deterministic framework will directly be used in Section 3 for implementing uncertainties in a nonparametric probabilistic framework. The boundary value problem (that is formulated in the frequency domain) is introduced for linear viscoelastic composite structures and its weak formulation is given in order to derive the computational model. Finally, the deterministic reduced-order computational model is constructed.

2.1. Boundary value problem for composite structures in the frequency domain

Let $\Omega = \Omega_e \cup \Omega_{ve}$ be an open, connected, and bounded domain of $\mathbb{R}^3$, constituted of two parts Ω_e and Ω_{ve}. The first part Ω_e is occupied by a purely elastic medium while the second part Ω_{ve} is occupied by a linear viscoelastic medium. It should be noted that the elastic medium Ω_e could be replaced by a viscoelastic medium without memory or by an elastic medium with an arbitrary damping model. In a cartesian frame $(\mathbf{e}_1, \mathbf{e}_2, \mathbf{e}_3)$, let $\mathbf{x} = (x_1, x_2, x_3)$ be the position vector of any point in Ω and $d\mathbf{x} = dx_1 dx_2 dx_3$ be the volume element. Let $\mathbf{n}$ be the external unit normal to the boundary $\partial\Omega$ of Ω, which is written as $\partial\Omega = \Gamma_u \cup \Gamma_f$, which is made of a part Γ_u on which a zero Dirichlet condition is imposed and a part Γ_f on which a surface force field, $\mathbf{f}_s(\mathbf{x}, t)$, is given. Let $\mathbf{u}(\mathbf{x}, t)$ be the displacement field defined on Ω. The linearized strain tensor is denoted by $\{\varepsilon_{kh}\}_{hk}$ and the Cauchy stress tensor by $\{\sigma_{ij}\}_{ij}$, with i, j, k, and h in $\{1, 2, 3\}$. Let $\rho(\mathbf{x})$ be the mass density of the composite structure. In the frequency domain, the boundary value problem is written, for all real ω belonging to the frequency band of analysis $B = [-\omega_{\lim}, \omega_{\lim}]$, as

$$-\omega^2 \rho(\mathbf{x})\, \widehat{\mathbf{u}}(\mathbf{x}, \omega) - \mathbf{div}\, \sigma(\widehat{\mathbf{u}}(\mathbf{x}, \omega)) = 0 \quad , \quad \text{in } \Omega \quad , \tag{1}$$

$$\widehat{\mathbf{u}}(\mathbf{x}, \omega) = \mathbf{0} \quad , \quad \text{on } \Gamma_u \quad , \tag{2}$$

$$\sigma(\widehat{\mathbf{u}}(\mathbf{x}, \omega))\, \mathbf{n} = \widehat{\mathbf{f}}_s(\mathbf{x}, \omega) \quad , \quad \text{on } \Gamma_f \quad . \tag{3}$$

This system of equations is then closed by a set of constitutive equations, which is detailed in the next subsections, and the dependence of the stress tensor σ with $\widehat{\mathbf{u}}(\mathbf{x},\omega)$ is denoted (using an abuse of notation) by $\sigma(\widehat{\mathbf{u}}(\mathbf{x},\omega))$.

2.2. Linear elastic constitutive equation for subdomain Ω_e

For all $\mathbf{x} \in \Omega_e$, the material is considered to be purely elastic, and as such we have the following constitutive equation

$$\sigma(\widehat{\mathbf{u}}(\mathbf{x},\omega)) = a^{elas}(\mathbf{x}) : \varepsilon(\widehat{\mathbf{u}}(\mathbf{x},\omega))\,, \tag{4}$$

in which the symbol " : " stands for the double inner tensor product, where the strain tensor is written as

$$\varepsilon_{kh}(\widehat{\mathbf{u}}(\mathbf{x},\omega)) = \frac{1}{2}\Big(\frac{\partial \widehat{u}_k(\mathbf{x},\omega)}{\partial x_h} + \frac{\partial \widehat{u}_h(\mathbf{x},\omega)}{\partial x_k}\Big)\,,$$

and where $\{a^{elas}_{ijkh}\}_{ijkh}$ is the fourth-order elasticity tensor that verifies the usual properties of symmetry, positivity, and boundness.

2.3. Linear viscoelastic constitutive equation for subdomain Ω_{ve}

The theory of linear viscoelasticity is used in order to obtain the constitutive equation of the viscoelastic medium occupied by domain Ω_{ve}. In all Section 2.3, $\mathbf{x}$ is fixed in Ω_{ve}.

Constitutive equation in the time domain. For $t \leq 0$, the system is assumed to be at rest,

$$\sigma(\mathbf{u}(\mathbf{x},t)) = 0 \quad , \quad \varepsilon(\mathbf{u}(\mathbf{x},t)) = 0 \quad , \quad \forall\, t \leq 0. \tag{5}$$

In the time domain, the constitutive equation is written as

$$\sigma(\mathbf{u}(\mathbf{x},t)) = \int_0^t \mathcal{G}(\mathbf{x},\tau) : \varepsilon(\dot{\mathbf{u}}(\mathbf{x},t-\tau))d\tau\ , \tag{6}$$

in which $\dot{\mathbf{u}}$ is the partial derivative of $\mathbf{u}$ with respect to t, where $t \mapsto \mathcal{G}(\mathbf{x},t)$ is the relaxation function defined on $[0\,+\infty[$ with values in the fourth-order tensor that satisfies the usual symmetry properties. Function $t \mapsto \mathcal{G}(\mathbf{x},t)$ is differentiable with respect to t on $]0,+\infty[$ and its partial time derivative $t \mapsto \{\dot{\mathcal{G}}_{ijkh}(\mathbf{x},t)\}_{ijkh}$ is assumed to be integrable on $[0\,,+\infty[$. At time $t = 0$, the initial elasticity tensor $\mathcal{G}(\mathbf{x},0)$ is positive definite. Using Eq. (5) and performing an integration by part, Eq. (6) can be rewritten as

$$\sigma(\mathbf{u}(\mathbf{x},t)) = \mathcal{G}(\mathbf{x},0) : \varepsilon(\mathbf{u}(\mathbf{x},t)) \,+\, \int_0^t \dot{\mathcal{G}}(\mathbf{x},\tau) : \varepsilon(\mathbf{u}(\mathbf{x},t-\tau))dt\,. \tag{7}$$

Let us introduce the fourth-order tensor $g(\mathbf{x},t)$ defined by

$$g(\mathbf{x},t) = 0 \quad \text{if } t < 0\,, \tag{8}$$

$$g(\mathbf{x},t) = \dot{\mathcal{G}}(\mathbf{x},t) \quad \text{if } t \geq 0\,. \tag{9}$$

From Eqs. (5), (8), and Eq. (9), it can be deduced that Eq. (7) can be rewritten as

$$\sigma(\mathbf{u}(\mathbf{x},\mathbf{t})) = \mathcal{G}(\mathbf{x},0) : \varepsilon(\mathbf{u}(\mathbf{x},t)) \; + \; \int_{-\infty}^{+\infty} g(\mathbf{x},\tau) : \varepsilon(\mathbf{u}(\mathbf{x},t-\tau))dt \; . \qquad (10)$$

Constitutive equation in the frequency domain. Taking the Fourier transform with respect to t of both sides of Eq. (10), and introducing the real part $\widehat{g}^R(\mathbf{x},\omega) = \Re e\{\widehat{g}(\mathbf{x},\omega)\}$ and the imaginary part $\widehat{g}^I(\mathbf{x},\omega) = \Im m\{\widehat{g}(\mathbf{x},\omega)\}$, the constitutive equation in the frequency domain can be written as

$$\sigma(\widehat{\mathbf{u}}(\mathbf{x},\omega)) = (a(\mathbf{x},\omega) + \mathrm{i}\,\omega\, b(\mathbf{x},\omega)) : \varepsilon(\widehat{\mathbf{u}}(\mathbf{x},\omega))\,, \qquad (11)$$

where the components $a_{ijkh}(\mathbf{x},\omega)$ and $b_{ijkh}(\mathbf{x},\omega)$ of the fourth-order real tensors $a(\mathbf{x},\omega)$ and $b(\mathbf{x},\omega)$ are the viscoelastic coefficients that are such that

$$a(\mathbf{x},\omega) = \mathcal{G}(\mathbf{x},0) + \widehat{g}^R(\mathbf{x},\omega) \quad , \quad \omega\, b(\mathbf{x},\omega) = \widehat{g}^I(\mathbf{x},\omega)\,. \qquad (12)$$

Properties of $\{a_{ijkh}(\mathbf{x},\omega)\}_{ijkh}$ *and* $\{b_{ijkh}(\mathbf{x},\omega)\}_{ijkh}$. The viscoelastic coefficients $a_{ijkh}(\mathbf{x},\omega)$ and $b_{ijkh}(\mathbf{x},\omega)$ of the fourth-order real tensors $a(\mathbf{x},\omega)$ and $b(\mathbf{x},\omega)$ are frequency dependent and exhibit several important properties [22, 24, 7], which have to be taken into account for a stochastic modeling (even functions with respect to ω, symmetry and positive definiteness properties). For all fixed $\mathbf{x}$ and ω, tensors $a(\mathbf{x},\omega)$ and $b(\mathbf{x},\omega)$ are such that:
(i) The tensors are even functions with respect to ω,

$$a(\mathbf{x},-\omega) = a(\mathbf{x},\omega) \quad , \quad b(\mathbf{x},-\omega) = b(\mathbf{x},\omega)\,; \qquad (13)$$

(ii) The symmetry property of the tensors is written as

$$a_{ijkh}(\mathbf{x},\omega) = a_{jikh}(\mathbf{x},\omega) = a_{ijhk}(\mathbf{x},\omega) = a_{khij}(\mathbf{x},\omega)\,, \qquad (14)$$

$$b_{ijkh}(\mathbf{x},\omega) = b_{jikh}(\mathbf{x},\omega) = b_{ijhk}(\mathbf{x},\omega) = b_{khij}(\mathbf{x},\omega)\,; \qquad (15)$$

(iii) The positiveness property of the tensors are such that, for all second-order real symmetric tensors $\{X_{ij}\}_{ij}$, there is a positive real constant c_0 independent of ω, such that

$$a_{ijkh}(\mathbf{x},\omega)X_{ij}X_{kh} \geq c_0 X_{ij}X_{ij} \quad , \quad b_{ijkh}(\mathbf{x},\omega)X_{ij}X_{ij} \geq c_0 X_{ij}X_{kh}\,, \qquad (16)$$

in which the classical convention for summations over repeated Latin indices is used.

Relations on the viscoelastic coefficients induced by the causality. Since g is a causal function of time, the real part $\widehat{g}^R$ and imaginary part $\widehat{g}^I$ of its Fourier transform $\widehat{g}$ are related through a set of compatibility equations also known as the Kramers-Kronig relations [25, 26]. These relations involve the Hilbert transform [27] and are written as

$$\widehat{g}^R(\mathbf{x},\omega) = \frac{1}{\pi}\, p.v \int_{-\infty}^{+\infty} \frac{\widehat{g}^I(\mathbf{x},\omega')}{\omega-\omega'}\, d\omega', \qquad (17)$$

$$\widehat{g}^I(\mathbf{x},\omega) = -\frac{1}{\pi}\, p.v \int_{-\infty}^{+\infty} \frac{\widehat{g}^R(\mathbf{x},\omega')}{\omega-\omega'} d\omega', \tag{18}$$

in which $p.v$ denotes the Cauchy principal value. For any function h that is integrable over the real line except at a singularity point ω given in $\mathbb{R}$, the $p.v$ is defined as

$$p.v \int_{-\infty}^{+\infty} h(\omega')\, d\omega' = \lim_{\zeta\to+\infty,\eta\to 0^+} \{ \int_{-\zeta}^{\omega-\eta} h(\omega')\, d\omega' + \int_{\omega+\eta}^{\zeta} h(\omega')\, d\omega' \}\,. \tag{19}$$

It should be noted that Eqs. (17) and (18) are equivalent and consequently, only one from these two equations can be used. From Eqs. (12) and (17), the following equation between the viscoelastic tensors $a(\mathbf{x},\omega)$ and $b(\mathbf{x},\omega)$ can be deduced

$$a(\mathbf{x},\omega) = a(\mathbf{x},0) + \frac{\omega}{\pi}\, p.v \int_{-\infty}^{+\infty} \frac{b(\mathbf{x},\omega')}{\omega-\omega'}\, d\omega' \quad , \quad \forall\, \omega \geq 0\,. \tag{20}$$

As $b(\mathbf{x},\omega')$ is an even function in ω', Eq. (20) can be rewritten as

$$a(\mathbf{x},\omega) = a(\mathbf{x},0) + \frac{2\,\omega^2}{\pi}\, p.v \int_{0}^{+\infty} \frac{b(\mathbf{x},\omega')}{\omega^2-\omega'^2} d\omega' \quad , \quad \forall\, \omega \geq 0\,. \tag{21}$$

For computational purposes, it is of interest to fix the position of the singularity. The change of variable $\omega' = \omega\, u$ yields

$$a(\mathbf{x},\omega) = a(\mathbf{x},0) + \frac{2\,\omega}{\pi}\, p.v \int_{0}^{+\infty} \frac{b(\mathbf{x},\omega\, u)}{1-u^2}\, du\,, \tag{22}$$

where the singularity is fixed at $u = 1$. The values for $\omega < 0$ are deduced using $a(\mathbf{x},\omega) = a(\mathbf{x},-\omega)$. This relation implies that, in the context of linear viscoelasticity, tensor-valued functions $\omega \mapsto a(\mathbf{x},\omega)$ and $\omega \mapsto b(\mathbf{x},\omega)$ cannot be chosen arbitrarily and have to verify Eq. (22) in order to satisfy the causality principle.

2.4. Rewriting the constitutive equation on domain $\Omega = \Omega_e \cup \Omega_{ve}$

By defining the fourth-order tensors $\mathbb{a}(\mathbf{x},\omega)$ and $\mathbb{b}(\mathbf{x},\omega)$ by

$$\mathbb{a}(\mathbf{x},\omega) = \begin{cases} a^{elas}(\mathbf{x}) & \forall \mathbf{x} \in \Omega_e\ , \\ a(\mathbf{x},\omega) & \forall \mathbf{x} \in \Omega_{ve}\ , \end{cases} \tag{23}$$

$$\mathbb{b}(\mathbf{x},\omega) = \begin{cases} 0 & \forall \mathbf{x} \in \Omega_e\ , \\ b(\mathbf{x},\omega) & \forall \mathbf{x} \in \Omega_{ve}\ , \end{cases} \tag{24}$$

and using Eqs. (4) and (11), the constitutive equation can be written, for all $\mathbf{x} \in \Omega$, as

$$\sigma(\widehat{\mathbf{u}}(\mathbf{x},\omega)) = (\mathbb{a}(\mathbf{x},\omega) + i\omega\, \mathbb{b}(\mathbf{x},\omega)) : \varepsilon(\widehat{\mathbf{u}}(\mathbf{x},\omega))\,. \tag{25}$$

2.5. Weak formulation of the boundary value problem

Let $\mathcal{C}_{ad}$ be a set of $\mathbb{C}^3$-valued functions defined on Ω that are sufficiently differentiable (it is the complex Sobolev space $(H^1(\Omega))^3$) and let $\mathcal{C}_0^{ad}$ be the admissible set such that $\mathcal{C}_0^{ad} = \{\mathbf{v} \in \mathcal{C}_{ad}\,,\, \mathbf{v} = \mathbf{0} \text{ on } \Gamma_u\}$. The weak formulation of the boundary value problem defined by Eqs. (1) to (3) with Eqs. (22) and (25) consists, for all ω fixed in B, in finding the function $\{\mathbf{x} \mapsto \widehat{\mathbf{u}}(\mathbf{x},\omega)\} \in \mathcal{C}_0^{ad}$ such that, for all $\mathbf{v} \in \mathcal{C}_0^{ad}$,

$$-\omega^2\, m(\widehat{\mathbf{u}},\mathbf{v}) \,+\, i\omega\, d(\widehat{\mathbf{u}},\mathbf{v};\omega) \,+\, k_0(\widehat{\mathbf{u}},\mathbf{v}) \,+ k(\widehat{\mathbf{u}},\mathbf{v};\omega) = f(\mathbf{v};\omega)\,, \tag{26}$$

in which

$$m(\widehat{\mathbf{u}},\mathbf{v}) = \int_\Omega \rho(\mathbf{x})\, \widehat{\mathbf{u}}\cdot\mathbf{v}\, d\mathbf{x}\,, \tag{27}$$

$$d(\widehat{\mathbf{u}},\mathbf{v};\omega) = \int_\Omega \{\mathbb{b}(\mathbf{x},\omega) : \varepsilon(\widehat{\mathbf{u}})\} : \varepsilon(\mathbf{v})\, d\mathbf{x}\,. \tag{28}$$

$$k_0(\widehat{\mathbf{u}},\mathbf{v}) = \int_\Omega \{\mathbb{c}_0(\mathbf{x}) : \varepsilon(\widehat{\mathbf{u}})\} : \varepsilon(\mathbf{v})\, d\mathbf{x}\,, \tag{29}$$

$$k(\widehat{\mathbf{u}},\mathbf{v};\omega) = \frac{2\,\omega}{\pi}\, p.v \int_0^{+\infty} \frac{d(\widehat{\mathbf{u}},\mathbf{v};\omega\, u)}{1-u^2}\, du\,. \tag{30}$$

$$f(\mathbf{v};\omega) = \int_{\Gamma_f} \widehat{\mathbf{f}}_s(\mathbf{x},\omega)\cdot\mathbf{v}\, ds(\mathbf{x})\,, \tag{31}$$

where $ds(\mathbf{x})$ is the surface element on Γ_f and where $\mathbb{c}_0(\mathbf{x}) = \mathbb{c}(\mathbf{x},0)$. It should be noted that, if there is an instantaneous linear viscoelastic medium in Ω_{ve}, then $\mathbb{b}(\mathbf{x},\omega) = \mathbb{b}(\mathbf{x})$ is independent of ω, which yields $d(\widehat{\mathbf{u}},\mathbf{v};\omega) = \int_{\Omega_{ve}} \{b(\mathbf{x}) : \varepsilon(\widehat{\mathbf{u}})\} : \varepsilon(\mathbf{v})\, d\mathbf{x}$, and since $p.v\, \int_0^{+\infty}(1-u^2)^{-1} du = 0$, then $k(\widehat{\mathbf{u}},\mathbf{v};\omega) = 0$.

2.6. Computational model

Applying the standard finite element method (see for instance [35, 36]) to Eq. (26) yields the computational model

$$(-\omega^2[\mathbb{M}] + i\omega[\mathbb{D}(\omega)] + [\mathbb{K}_0] + [\mathbb{K}(\omega)])\,\widehat{\mathbb{u}}(\omega) = \widehat{\mathbb{f}}(\omega)\,, \tag{32}$$

in which $\widehat{\mathbb{u}}(\omega)$ is the complex vector of the degrees of freedom, and where $\widehat{\mathbb{f}}(\omega)$, $[\mathbb{M}]$, $[\mathbb{D}(\omega)]$, $[\mathbb{K}_0]$, and $[\mathbb{K}(\omega)]$ correspond to the finite element discretization of f, m, d, k_0 and k respectively. The symmetric positive real matrix $[\mathbb{K}(\omega)]$ is such that

$$[\mathbb{K}(\omega)] = \frac{2\,\omega}{\pi}\, p.v \int_0^{+\infty} \frac{[\mathbb{D}(\omega u)]}{1-u^2}\, du\,. \tag{33}$$

It is assumed that domains Ω_e and Ω_{ve} that constitute Ω are such that the symmetric real matrix $[\mathbb{K}_0]$ is positive definite. In order to later implement the nonparametric probabilistic approach as well as to reduce the computational cost for solving the computational model, a reduced-order computational model is introduced.

2.7. Reduced-order computational model

As suggested in [7], the reduced-order computational model is constructed by using the reduced basis represented by the rectangular real matrix $[\Phi_N]$ whose N columns are the first N modes associated with the first N positive eigenvalues $0 < \omega_1^2 \leq \ldots \leq \omega_N^2$ of the underlying undamped mechanical system for which the mass matrix is $[\mathbb{M}]$ and the stiffness matrix is $[\mathbb{K}_0]$. Consequently, the $(N \times N)$ real matrices $[\mathcal{M}]$ and $[\mathcal{K}_0]$, which are defined by

$$[\mathcal{M}] = [\Phi_N]^T [\mathbb{M}][\Phi_N] \quad , \quad [\mathcal{K}_0] = [\Phi_N]^T [\mathbb{K}_0][\Phi_N] \, , \tag{34}$$

are diagonal, positive definite, and $[\mathcal{K}_0]_{pp} = \omega_p^2 \, [\mathbb{M}]_{pp}$. The reduced-order computational model is then written as

$$\widehat{\mathbb{u}}^{(N)}(\omega) = [\Phi_N] \, \widehat{\mathbf{q}}(\omega) \, , \tag{35}$$

$$(-\omega^2 [\mathcal{M}] + i\omega \, [\mathcal{D}(\omega)] + [\mathcal{K}_0] + [\mathcal{K}(\omega)]) \, \widehat{\mathbf{q}}(\omega) = \widehat{\mathbf{f}}(\omega) \, , \tag{36}$$

in which $\widehat{\mathbf{f}}(\omega) = [\Phi_N]^T \, \widehat{\mathbb{f}}(\omega)$ and where the full $(N \times N)$ real matrices $[\mathcal{D}(\omega)] = [\Phi_N]^T [\mathbb{D}(\omega)][\Phi_N]$ and $[\mathcal{K}(\omega)] = [\Phi_N]^T [\mathbb{K}(\omega)][\Phi_N]$ are symmetric positive, and are linked by the following equation,

$$[\mathcal{K}(\omega)] = \frac{2\,\omega}{\pi} \; p.v \int_0^{+\infty} \frac{1}{1-u^2} [\mathcal{D}(\omega u)] \, du \quad , \quad \omega \geq 0 \, . \tag{37}$$

A convergence analysis is carried out in order to determine the value of N such that $\widehat{\mathbb{u}}(\omega) \approx \widehat{\mathbb{u}}^{(N)}(\omega)$ for all ω in frequency band B. It is assumed that the basis $[\Phi_N]$ is such that for all $\omega \geq 0$, matrix $[\mathcal{D}(\omega)]$ is positive definite and matrix $[\mathcal{K}(\omega)]$ is positive or positive definite.

3. Stochastic reduced-order computational model

For N fixed as explained before, the nonparametric probabilistic approach of uncertainties consists in substituting in Eqs. (36) and (37), the deterministic matrices $[\mathcal{M}]$, $[\mathcal{D}(\omega)]$, $[\mathcal{K}_0]$, and $[\mathcal{K}(\omega)]$, by the $(N \times N)$ real random matrices $[\mathbf{M}]$, $[\mathbf{D}(\omega)]$, $[\mathbf{K}_0]$, and $[\mathbf{K}(\omega)]$ respectively, in preserving the positive-definiteness property of $[\mathbf{M}]$, $[\mathcal{D}(\omega)]$, $[\mathbf{K}_0]$, and the positiveness property of $[\mathbf{K}(\omega)]$. Consequently $\widehat{\mathbf{q}}(\omega)$ and $\widehat{\mathbb{u}}^{(N)}(\omega)$ become the random vectors $\widehat{\mathbf{Q}}(\omega)$ and $\widehat{\mathbb{U}}^{(N)}(\omega)$ such that

$$\widehat{\mathbb{U}}^{(N)}(\omega) = [\Phi_N] \, \widehat{\mathbf{Q}}(\omega) \, , \tag{38}$$

$$(-\omega^2 [\mathbf{M}] + i\omega \, [\mathbf{D}(\omega)] + [\mathbf{K}_0] + [\mathbf{K}(\omega)]) \, \widehat{\mathbf{Q}}(\omega) = \widehat{\mathbf{f}}(\omega) \, , \tag{39}$$

$$[\mathbf{K}(\omega)] = \frac{2\,\omega}{\pi} \; p.v \int_0^{+\infty} \frac{1}{1-u^2} [\mathbf{D}(\omega u)] \, du \quad , \quad \omega \geq 0 \, . \tag{40}$$

It should be noted that Eq. (40) means that the probabilistic model of random matrix $[\mathbf{K}(\omega)]$ is completely defined by the probabilistic model of random matrix $[\mathbf{D}(\omega)]$. We then obtain a probabilistic model for random matrix $[\mathbf{K}(\omega)]$

which satisfies almost-surely the causality principle. Hereinafter, this probabilistic model is referred to as the probabilistic model with almost-sure causality. Consequently, only the probabilistic models of random matrices $[\mathbf{M}]$, $[\mathbf{K}_0]$ and $[\mathbf{D}(\omega)]$ have to be constructed. In the framework of the nonparametric probabilistic approach of uncertainties, these random matrices are constructed as explained in [2, 5, 6]. These random matrices are statistically independent and are defined by

$$[\mathbf{M}] = [\underline{L}_M]^T [\mathbf{G}_M] [\underline{L}_M] , \tag{41}$$

$$[\mathbf{K}_0] = [\underline{L}_{K_0}]^T [\mathbf{G}_K] [\underline{L}_{K_0}] , \tag{42}$$

$$[\mathbf{D}(\omega)] = [\underline{L}_D(\omega)]^T [\mathbf{G}_D] [\underline{L}_D(\omega)] . \tag{43}$$

in which $[\underline{L}_M]$, $[\underline{L}_{K_0}]$, and $[\underline{L}_D(\omega)]$ are the deterministic upper triangular matrices such that

$$[\mathcal{M}] = [\underline{L}_M]^T [\underline{L}_M] \quad , \quad [\mathcal{K}_0] = [\underline{L}_{K_0}]^T [\underline{L}_{K_0}] \quad , \quad [\mathcal{D}(\omega)] = [\underline{L}_D(\omega)]^T [\underline{L}_D(\omega)] .$$

The random matrices $[\mathbf{G}_M]$, $[\mathbf{G}_K]$, and $[\mathbf{G}_D]$ are positive-definite $(N \times N)$ real random matrices that are statistically independent, which are defined by

$$[\mathbf{G}_M] = [\mathbf{L}_{G_M}]^T [\mathbf{L}_{G_M}] \quad , \quad [\mathbf{G}_K] = [\mathbf{L}_{G_K}]^T [\mathbf{L}_{G_K}] \quad , \quad [\mathbf{G}_D] = [\mathbf{L}_{G_D}]^T [\mathbf{L}_{G_D}] ,$$

in which the upper triangular random matrices $[\mathbf{L}_{G_M}]$, $[\mathbf{L}_{G_K}]$, and $[\mathbf{L}_{G_D}]$ are defined by

$$[\mathbf{L}_{G_M}]_{jj'} = \sigma(\delta_M)\, V^M_{jj'} \quad , \quad [\mathbf{L}_{G_M}]_{jj} = \sigma(\delta_M) \sqrt{2h(\alpha_j(\delta_M), V^M_{jj})} , \tag{44}$$

$$[\mathbf{L}_{G_K}]_{jj'} = \sigma(\delta_K)\, V^K_{jj'} \quad , \quad [\mathbf{L}_{G_K}]_{jj} = \sigma(\delta_K) \sqrt{2h(\alpha_j(\delta_K), V^K_{jj})} , \tag{45}$$

$$[\mathbf{L}_{G_D}]_{jj'} = \sigma(\delta_D)\, V_{jj'} \quad , \quad [\mathbf{L}_{G_D}]_{jj} = \sigma(\delta_D) \sqrt{2h(\alpha_j(\delta_D), V^D_{jj})} , \tag{46}$$

in which $\{V^M_{jj'}, V^K_{jj'}, V^D_{jj'} , 1 \leq j \leq j' \leq N\}$ is a set of independent real-valued normalized Gaussian random variables. The real parameters σ and α_j depend on a hyperparameter δ such that $0 < \delta < (\frac{N+1}{N+5})^{\frac{1}{2}}$ and are defined by $\sigma(\delta) = \delta(N+1)^{-\frac{1}{2}}$ and $\alpha_j(\delta) = \frac{N+1}{2\delta^2} + \frac{1-j}{2}$. The function $h(\alpha, V)$ is written as $h(\alpha, V) = F^{-1}_{\Gamma_\alpha}(F_V(v))$ where F_V and F_{Γ_α} are the cumulative distribution functions of a standard Gaussian random variable V and a Gamma random variable Γ_α with parameter α. The hyperparameters δ_M, δ_K, and δ_D allow for controling the level of uncertainties for each matrix of the reduced-order computational model.

Remarks.

- With the stochastic construction defined by Eq. (40), it must be verified that, for all $\omega \geq 0$, $[\mathbf{K}(\omega)]$ is a positive-definite random matrix. In [6], it is proven the following sufficient condition. If for all real vector $\mathbf{y} = (y_1, \ldots, y_N)$, the random function $\omega \mapsto \mathbf{y}^T [\mathbf{D}(\omega)] \mathbf{y}$ is decreasing in ω for $\omega \geq 0$, then, for all $\omega \geq 0$, $[\mathbf{K}(\omega)]$ is a positive-definite random matrix.

- If the causality principle was not taken into account for the construction of the stochastic model of random matrix $[\mathbf{K}(\omega)]$, then the stochastic model that would be constructed would be causal in average but would not be almost-surely causal. Such a model that would be causal only in mean, would be erroneous from the point of view of the theory of physically realizable systems. In the following, such an erroneous stochastic construction will be referred as the probabilistic model with a causality in mean. Such a model can be constructed by rewriting Eq. (39) as

$$([\mathbf{M}] + i\omega[\mathbf{D}(\omega)] + [\widetilde{\mathbf{K}}(\omega)])\,\widehat{\mathbf{Q}}(\omega) = \widehat{\mathbf{f}}(\omega)\,, \tag{47}$$

where $[\widetilde{\mathbf{K}}(\omega)] = [\mathbf{K}_0] + [\mathbf{K}(\omega)]$. The random matrices $[\mathbf{M}]$ and $[\mathbf{D}(\omega)]$ are constructed as previously, but now the probabilistic model of the random matrix $[\widetilde{\mathbf{K}}(\omega)]$ would be written as

$$[\widetilde{\mathbf{K}}(\omega)] = [\underline{L}_{\widetilde{K}}(\omega)]^T [\mathbf{G}_K] [\underline{L}_{\widetilde{K}}(\omega)]\,, \tag{48}$$

where $[\underline{L}_{\widetilde{K}}(\omega)]$ corresponds to the Cholesky factorization of the positive-definite random matrix $[\widetilde{\mathcal{K}}(\omega)] = [\mathcal{K}_0] + [\mathcal{K}(\omega)]$.

4. Computational aspects

4.1. Computation of the Hilbert transform

The computation of statistically independent realizations of random matrix $[\mathbf{K}(\omega)]$ using Eq. (40) can be tricky. It requires the knowledge of the function $\omega \mapsto [\mathbf{D}(\omega)]$ for all $\omega \geq 0$ and not only on the frequency band B of analysis. A first naive approach would be to truncate the infinite interval of integration in order to obtain a finite interval. Such an approximation would require that each entry of matrix $[\mathbf{D}(\omega)]$ decreases fast enough when ω increases, which might not be the case in the presence of strongly dissipative materials. To circumvent this problem, the integral in Eq. (40) is split into two integrals, one over $[0, u_g]$ and another one over $[u_g, +\infty[$, where u_g should be greater than 1,

$$[\mathbf{K}(\omega)] = \frac{2\omega}{\pi}\{\,[\mathbf{I}_1(\omega)] + [\mathbf{I}_2(\omega)]\,\}\,, \tag{49}$$

where the two random matrices $[\mathbf{I}_1(\omega)]$ and $[\mathbf{I}_2(\omega)]$ are such that

$$[\mathbf{I}_1(\omega)] = p.v \int_0^{u_g} \frac{1}{1-u^2}[\mathbf{D}(\omega u)]du\,, \tag{50}$$

$$[\mathbf{I}_2(\omega)] = \int_{u_g}^{+\infty} \frac{1}{1-u^2}[\mathbf{D}(\omega u)]du\,. \tag{51}$$

For computing random matrix $[\mathbf{I}_1(\omega)]$, which involves an integration on an interval that includes a singularity at $u = 1$, the integrand is evaluated for a high number of values of u and a trapezoidal rule with N_u points is used. For materials that are strongly dissipative over a large frequency band, that is, when

the entries of matrix $[\mathbf{D}(\omega)]$ are slowly decreasing with ω, the computation of random matrix $[\mathbf{I}_2(\omega)]$ can be costly if a standard Newton-Cotes integration scheme over a truncated finite interval $[u_g, a]$ is used with a large upper bound a. For this purpose, the integration over $[u_g, +\infty[$ is rewritten as an integration over $[-1, 1]$ using a change of variable and then, an *ad hoc* Gaussian quadrature rule is introduced to compute $[\mathbf{I}_2(\omega)]$ with a very small number N_q of quadrature points. The details concerning the computation of $[\mathbf{I}_1(\omega)]$ are given in Section 4.1.1 and those concerning the computation of $[\mathbf{I}_2(\omega)]$, notably the construction of the quadrature rule, are given in Section 4.1.2.

4.1.1. Computation of random matrix $[\mathbf{I}_1(\omega)]$

Section 4.1.1 is devoted to the numerical method adopted to compute $[\mathbf{I}_1(\omega)]$, which is written as

$$[\mathbf{I}_1(\omega)] = \lim_{\eta \to 0^+} \{ \int_0^{1-\eta} \frac{1}{1-u^2} [\mathbf{D}(\omega u)]\, du + \int_{1+\eta}^{u_g} \frac{1}{1-u^2} [\mathbf{D}(\omega u)]\, du \}\,, \qquad (52)$$

in which the constant $u_g > 1$ can arbitrarily be chosen. The limit $\eta \to 0^+$ is taken into account by sampling the values of the integrand at the sampling points $\{u_i\,,\, i = 1, \ldots, N_u\,,\, u_i \neq 1\}$ with a constant step $u_{i+1} - u_i \ll 1$ of the interval $[0, u_g]$. The use of a trapezoidal integration rule yields

$$[\mathbf{I}_1(\omega)] = \sum_{i=1}^{N_u - 1} (\frac{u_{i+1} - u_i}{2})(\frac{[\mathbf{D}(\omega u_i)]}{1-u_i^2} + \frac{[\mathbf{D}(\omega u_{i+1})]}{1-u_{i+1}^2})\,. \qquad (53)$$

4.1.2. Computation of random matrix $[\mathbf{I}_2(\omega)]$

Section 4.1.2 deals with the numerical method adopted to compute

$$[\mathbf{I}_2(\omega)] = \int_{u_g}^{+\infty} \frac{1}{1-u^2}\, [\mathbf{D}(\omega u)] du\,, \qquad (54)$$

for materials that are strongly dissipative over a large frequency band, and for $u_g > 1$. As explained before, a change of variable and an *ad hoc* quadrature rule are introduced to compute $[\mathbf{I}_2(\omega)]$. The following change of variable $\eta \mapsto u = \mathcal{U}(\eta)$ from $[-1, 1[$ into $[u_g\,, +\infty[$ is introduced,

$$\mathcal{U}(\eta) = \frac{2\, u_g}{1-\eta} \quad , \quad u_g > 1\,. \qquad (55)$$

Eq. (54) can then be rewritten as

$$[\mathbf{I}_2(\omega)] = \mu \int_{-1}^{1} [\mathbf{D}(\omega\, \mathcal{U}(\eta))]\, p_H(\eta)\, d\eta\,, \qquad (56)$$

in which the negative real constant μ is defined by

$$\mu = \frac{1}{2} \log \frac{(u_g - 1)}{(u_g + 1)} < 0 \quad , \quad u_g > 1\,, \qquad (57)$$

and where p_H is a function defined on $[-1,1]$ with values in $\mathbb{R}^+$, such that

$$p_H(\eta) = \frac{2u_g}{\mu(\eta^2 - 2\eta + 1 - 4u_g^2)} \quad , \quad \eta \in [-1,1] \quad , \quad u_g > 1\,. \tag{58}$$

Positive-valued function p_H, which is such that

$$\int_{-1}^{1} p_H(\eta)\, d\eta = 1\,, \tag{59}$$

can then be viewed as the probability density function of a $[-1,1]$-valued random variable H defined on a probability space $(\Xi, \mathcal{T}, \mathcal{P})$ (this property will be used after). In the following, a N_q-points Gaussian quadrature rule with respect to the measure $p_H(\eta)\, d\eta$ on $[-1,1]$ is constructed and $[\mathbf{I}_2(\omega)]$ is then calculated by

$$[\mathbf{I}_2(\omega)] \approx \sum_{q=1}^{Nq} w_q [\mathbf{D}(\omega\, \mathcal{U}(\eta_q))]\,, \tag{60}$$

where η_q is the q-th Gauss point and w_q is its associated Gauss weight.

(i) Construction of the quadrature rule for the computation of $[\mathbf{I}_2(\omega)]$.
The procedure to construct the quadrature rule associated with any measure is detailed, for instance, by W. Gautschi in [31]. The construction is based on the three-term relation that can be expressed between monic polynomials (univariate polynomials in which the nonzero coefficient of highest degree is equal to 1) that are orthogonal with respect to measure $p_H(\eta)\, d\eta$ on $[-1,1]$. Let $\mathbb{H} = L^2_{p_H(\eta)d\eta}([-1,1])$ be the Hilbert space of all the square integrable real functions defined on $[-1,1]$ with respect to the probability measure $p_H(\eta)\, d\eta$, equipped with the inner product and the associated norm,

$$< g\,, g' >= \int_{-1}^{1} g(\eta)\, g'(\eta)\, p_H(\eta)\, d\eta \quad , \quad \|g\| =< g\,, g >^{1/2}\,. \tag{61}$$

For $k = 0, \ldots, N_q$, let $\pi_k(\eta)$ be the k-th order monic orthogonal polynomial in $\mathbb{H}$ with degree k. Consequently, for k and k' in $\{0, 1, \ldots, N_q\}$,

$$< \pi_k\,, \pi_{k'} >= 0 \quad \text{for} \quad k \neq k'\,. \tag{62}$$

The three-term relation between this family of orthogonal polynomials is written as

$$\pi_{k+1}(\eta) = (\eta - \alpha_k)\, \pi_k(\eta) - \beta_k\, \pi_{k-1}(\eta) \quad , \quad k = 0, 1, ..., N_q - 1\,, \tag{63}$$

$$\pi_0(\eta) = 1\ ,\ \pi_{-1}(\eta) = 0\,. \tag{64}$$

for which the coefficients α_k and β_k are written as

$$\alpha_k =< \eta\, \frac{\pi_k}{\|\pi_k\|}\,, \frac{\pi_k}{\|\pi_k\|} > \quad , \quad k = 0, ..., N_q - 1\,, \tag{65}$$

$$\beta_k = (\|\pi_k\| \, \|\pi_{k-1}\|^{-1})^2 \quad , \quad k = 1, ..., N_q - 1 \, . \tag{66}$$

in which $\|\pi_k\| \, \|\pi_{k-1}\|^{-1}$ can be calculated by the equation,

$$\|\pi_k\| \, \|\pi_{k-1}\|^{-1} = < \eta \, \frac{\pi_{k-1}}{\|\pi_{k-1}\|} \, , \frac{\pi_k}{\|\pi_k\|} > \quad , \quad k = 1, ..., N_q - 1 \, . \tag{67}$$

The value of the coefficient β_0 is arbitrary and defined by convention as

$$\beta_0 = \|\pi_0\|^2 = \int_{-1}^{1} p_H(\eta) \, d\eta = 1 \, . \tag{68}$$

Once the coefficients are known, one has to construct the following Jacobi matrix:

$$[J_{N_q}] = \begin{pmatrix} \alpha_0 & \sqrt{\beta_1} & & & \\ \sqrt{\beta_1} & \alpha_1 & \sqrt{\beta_2} & & \\ & \sqrt{\beta_2} & \alpha_2 & \sqrt{\beta_3} & \\ & & \ddots & \ddots & \ddots \\ & & & \sqrt{\beta_{N_q-1}} & \alpha_{N_q-1} \end{pmatrix} \tag{69}$$

The quadrature rule is then deduced by computing the eigenvalues $\eta_1, \ldots, \eta_{N_q}$ and the normalized eigenvectors $\mathbf{v}_1, \ldots, \mathbf{v}_{N_q}$ of this Jacobi matrix,

$$[J_{N_q}] \, \mathbf{v}_q = \eta_q \, \mathbf{v}_q \quad , \quad q = 1, \ldots, N_q \, . \tag{70}$$

The desired abscissa are $\eta_1, \ldots, \eta_{N_q}$ and the associated weights $w_1, \ldots, w_{N_q}$ are such that

$$w_q = \beta_0 \, \{\mathbf{v}_q\}_1^2 = \{\mathbf{v}_q\}_1^2 \quad , \quad q = 1, \ldots, N_q \, , \tag{71}$$

where $\{\mathbf{v}_q\}_1$ is the first component of the q-th normalized eigenvector $\mathbf{v}_q$.

It should be noted that, since the quadrature rule we constructed on $[-1, 1]$ is exact for polynomials of degree $2N_q - 1$ and because of Eq. (55), the integrands of the form $1/P(u)$, where $P(u)$ is a polynomial of degree $2N_q - 1$ at most, should be computed correctly.

(ii) Generation of orthogonal polynomials and computation of the coefficients α_k and β_k.

We thus have to construct the family of the monic orthogonal polynomials in $\mathbb{H}$. The Gram-Schmidt process is a common technique to generate a set of orthogonal polynomials from a starting set of polynomials (often taken as monomials of increasing order). However, this process is numerically unstable, especially as the number of polynomials to orthogonalize increases. In order to avoid such stability issues, we make use of an alternative method detailed in [34], which was successfully applied to the computation of polynomial chaos in high dimension with respect to an arbitrary measure. The method is numerically stable and is based on probability theory. Let us introduced the orthonormal polynomials $\{\Psi_0, \Psi_1, \ldots, \Psi_{N_q}\}$ associated with the orthogonal polynomials $\{\pi_0, \pi_1, \ldots, \pi_{N_q}\}$,

$$\Psi_k(\eta) = \pi_k(\eta) \|\pi_k\|^{-1} \quad , \quad k = 0, 1, \ldots, N_q - 1 \, , \tag{72}$$

Consequently, for all k and k' in $\{0, 1, \ldots, N_q - 1\}$, it can be deduced that

$$E\{\Psi_k(H)\,\Psi_{k'}(H)\} = \int_{-1}^{1} \Psi_k(\eta)\,\Psi_{k'}(\eta)\,p_H(\eta)\,d\eta = \delta_{kk'}\,, \tag{73}$$

in which E denotes the mathematical expectation and where $\delta_{kk'}$ is the Kronecker symbol. Let $H(\xi_1), \ldots, H(\xi_{n_s})$ be n_s independent realizations of random variable H with $\xi_1, \ldots, \xi_{n_s}$ in Ξ. These realizations are usually computed using the probability density function $p_H(\eta)$. For n_s sufficiently large, we have

$$E\{\Psi_k(H)\,\Psi_{k'}(H)\} \approx \frac{1}{n_s} \sum_{\ell=1}^{n_s} \Psi_k(H(\xi_\ell))\,\Psi_{k'}(H(\xi_\ell))\,. \tag{74}$$

Let $[\mathbb{P}]$ be the $(N_q \times n_s)$ real matrix such that

$$[\mathbb{P}]_{\kappa\ell} = \Psi_{\kappa-1}(H(\xi_\ell)) \quad , \quad \kappa = 1, \ldots, N_q \quad , \quad \ell = 1, \ldots, n_s\,. \tag{75}$$

It can then be deduced that

$$\lim_{n_s \to +\infty} \frac{1}{n_s - 1} [\mathbb{P}][\mathbb{P}]^T = [I_{N_q}]\,. \tag{76}$$

Let $[\mathbb{M}]$ be the $(N_q \times n_s)$ real matrix of realizations of the monomials such that

$$[\mathbb{M}]_{\kappa\ell} = H(\xi_\ell)^{\kappa-1} \quad , \quad \kappa = 1, \ldots, N_q \quad , \quad \ell = 1, \ldots, n_s\,. \tag{77}$$

The algorithm is then the following:

- Compute matrix $[\mathbb{M}]$ defined by Eq. (77), and then compute the $(N_q \times N_q)$ real matrix $[\mathbb{F}] = \frac{1}{n_s - 1}\,[\mathbb{M}]\,[\mathbb{M}]^T$. It is assumed that $n_s > N_q$ in order that matrix $[\mathbb{F}]$ is positive definite.
- Compute the lower triangular $(N_q \times N_q)$ real matrix $[\mathbb{L}]$ from the Cholesky decomposition $[\mathbb{L}]\,[\mathbb{L}]^T$ of positive-definite symmetric matrix $[\mathbb{F}]$.
- Compute the $(N_q \times n_s)$ real matrix $[\mathbb{P}]$ as the solution of the linear matrix equation $[\mathbb{L}]\,[\mathbb{P}] = [\mathbb{M}]$.

The coefficients α_k and β_k are calculated by using Eqs. (65) and (66) in which

$$< \eta\,\frac{\pi_k}{\|\pi_k\|}\,,\,\frac{\pi_k}{\|\pi_k\|} >= E\{H\,\Psi_k(H)^2\} \quad , \quad k = 0, ..., N_q - 1\,, \tag{78}$$

$$\|\pi_k\|\,\|\pi_{k-1}\|^{-1} = E\{H\,\Psi_{k-1}(H)\,\Psi_k(H)\} \quad , \quad k = 1, ..., N_q - 1\,. \tag{79}$$

for which, for $k = 0, ..., N_q - 1$, the following approximations are used,

$$E\{H\,\Psi_k(H)^2\} \approx \frac{1}{n_s} \sum_{\ell=1}^{n_s} H(\xi_\ell)\,\Psi_k(H(\xi_\ell))^2\,, \tag{80}$$

$$E\{H\,\Psi_{k-1}(H)\,\Psi_k(H)\} \approx \frac{1}{n_s} \sum_{\ell=1}^{n_s} H(\xi_\ell)\,\Psi_{k-1}(H(\xi_\ell))\,\Psi_k(H(\xi_\ell))\,. \tag{81}$$

4.2. Evaluation of the frequency-dependent matrices for a large number of frequency sampling points

As explained in Section 4.1, the numerical calculation of the integrals are performed by sampling the matrix-valued function $\omega \mapsto [\mathcal{D}(\omega)]$ for a large number of frequency points. A large number of construction and then of reduction of the damping matrix of the computational model can be computationally costly. We thus propose a way of sampling positive-definite matrices by interpolation. Such a method can be used for the purpose of performing the computation of the Hilbert transform. It can also be used to sample the frequency-dependent stiffness and damping matrices at a higher number of frequency points for the computation of the response of the system.

Interpolation method for positive-definite matrices. When the matrices are interpolated, one must worry about preserving their properties. In our case, we want to interpolate a function $x \mapsto [A(x)]$ with values in the set of all the symmetric positive-definite $(N \times N)$ real matrices. For that, the interpolation is performed on the upper triangular matrix coming from the Cholesky factorization as follows:

- Compute the upper triangular matrix $[L_A(x)]$ from the Cholesky factorization of matrix $[A(x)]$ at a number N_r of reference points $\{x_i^r, i = 1, ..., N_r\}$ using a regular or log-scale slicing.
- At each point x_j, $j = 1, ..., M$, where we want to interpolate, a component-by-component interpolation of $[L_A(x_j)]$ is performed with a Newton-Cotes formula, using the nearest points from set $\{x_i^r\}_i$.
- If necessary, the symmetric positive-definite matrix $[A(x_j)]$ is reconstructed using $[A(x_j)] = [L_A(x_j)]^T [L_A(x_j)]$.

The precision level of the interpolation is controlled directly by the number N_r of reference points x_i^r and their spacing.

4.3. Remarks concerning the stochastic solver and the parallel computing

The Monte Carlo method is used as a stochastic solver. Among its attributes, it should be noted that it is non-intrusive with respect to commercial software (black box) and that the speed of convergence can both be controlled during the computation and is independent of the dimension. Some advanced Monte Carlo procedures can also be employed in order to improve convergence speed (see for instance [37]). Such a stochastic solver is well-suited for massively parallel computing and consequently, can naturally be chosen as the first level of parallel computing. A second level of parallelization can easily be implemented for solving Eqs. (38) and (39) with respect to the sampled frequencies. Finally, a third level of parallelization can be considered for the calculation of Eqs. (53) and (60) related to the Hilbert transform for which the numerical cost is mainly due to the construction of the reduced-damping matrix. Nevertheless, as an interpolation approach is proposed, the gain given by such a third level of parallelization would stay small enough.

5. Numerical examples

Hereinafter, an example is given for which the proposed probabilistic model is carried out. The quantification of uncertainties is compared between two probabilistic approaches : *a*) for a model with almost-sure causality (the proposed model) and *b*) a model with causality in mean.

5.1. Description of the numerical model

The structure that is considered is a thin multilayered plate of length $L = 1$ m, width $W = 0.3$ m and thickness $H = 0.1$ m, under a nodal load of $F = 1$ N applied in direction $\mathbf{e}_3$ at the point located at (0.5067 m, 0.1565 m, 0.1 m) (see Fig. 1). The three layers are made up of a homogenous elastic medium occupying domain Ω_e that is sandwiched between two homogenous viscoelastic media occupying the domain $\Omega_{ve} = \Omega_1 \cup \Omega_2$ in which the domain Ω_1 is the upper layer and the domain Ω_2 is the lower layer. For the elastic medium, the material is assumed to be isotropic with Young's modulus $E = 210$ GPa, Poisson's ratio $\nu = 0.3$, and a density $\rho = 7,850$ kg/m^3. Its thickness is $h = 4H/5$ in which H is the total thickness of the plate. For the viscoelastic homogenous medium occupying domain Ω_k, with $k = 1, 2$, the material is assumed to be isotropic with a Poisson ratio $\nu^{(k)}$ and a time-dependent viscoelastic coefficient $E^{(k)}(t)$. Let $\widehat{E}^{(k)}(\omega)$ be the Fourier transform of $E^{(k)}(t)$. In the case of a single-branch generalized Maxwell model, we have

$$\widehat{E}_k(\omega) = E_\infty^{(k)} + \frac{E_1^{(k)}(\tau_1^{(k)}\omega)^2}{1+(\tau_1^{(k)}\omega)^2} + \mathrm{i}\,\omega\frac{E_1^{(k)}\tau_1^{(k)}}{1+(\tau_1^{(k)}\omega)^2}\ . \tag{82}$$

This makes use of rational functions for which the quadrature method presented earlier is exact. The viscoelastic coefficients used in the simulations are listed in Table 1.

	Upper layer k = 1	Lower layer k = 2
$\nu^{(k)}$	0.27	0.47
$E_\infty^{(k)}$ (GPa)	240	220
$E_1^{(k)}$ (GPa)	126.5	50
$\tau_1^{(k)}$ (s)	7.351×10^{-2}	1.103×10^{-1}

Table 1 Parameters of the single-branch generalized Maxwell model

5.1.1. Finite element model

The finite element mesh of the structure is constituted of 8-nodes 3D finite elements with 150 elements along direction $\mathbf{e}_1$ (length), 46 elements along $\mathbf{e}_2$ (thickness), and 21 elements along $\mathbf{e}_3$ (thickness). The total number of degrees of freedom is $468,402$. Figs. 1 and 2 show the finite element mesh of the structure.

The frequency response is analyzed in the frequency band of analysis $B_\nu = [0\,,400]$ Hz.

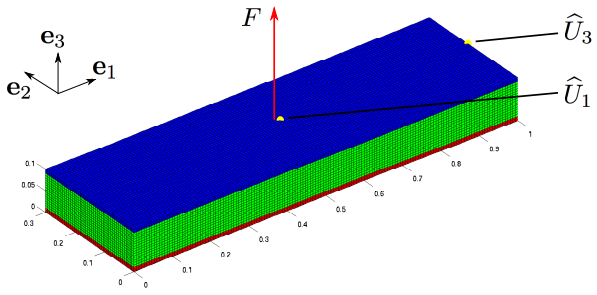

Figure 1 Finite element mesh of the plate with force applied $F = 1$ N and observation dofs $\widehat{U}_1$ and $\widehat{U}_3$. Angle of observation: azimuth $= -37.5°$, elevation $= 30°$

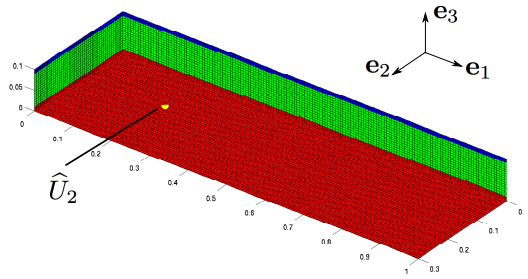

Figure 2 Finite element mesh of the plate with observation dof $\widehat{U}_2$. Angle of observation: azimuth $= -37.5°$, elevation $= -30°$

5.1.2. Quantification of the viscoelasticity effects on the stiffness of the computational model

In this section the viscoelasticity effects are analyzed on the stiffness of the computational model and are quantified by comparing the solutions $\widehat{\mathbf{q}}'(\omega)$ and $\widehat{\mathbf{q}}(\omega)$ of the following reduced-order computational models,

$$(-\omega^2[\mathcal{M}] + i\omega[\mathcal{D}(w)] + [\mathcal{K}_0])\,\widehat{\mathbf{q}}'(\omega) = \widehat{\mathbf{f}}(\omega)\,, \tag{83}$$

$$(-\omega^2[\mathcal{M}] + i\omega[\mathcal{D}(w)] + [\mathcal{K}_0] + [\mathcal{K}(\omega)])\,\widehat{\mathbf{q}}(\omega) = \widehat{\mathbf{f}}(\omega)\,, \tag{84}$$

for which $N = 400$, the eigenfrequencies being from about 3 Hz to about $1,100$ Hz. In Eq. (83), the generalized stiffness is $[\mathcal{K}_0]$ and does not include the additional frequency-dependent matrix $[\mathcal{K}(\omega)]$ which is related to the viscoelasticity of the materials in the upper and the lower layers. In Eq. (84), the additional frequency-dependent matrix $[\mathcal{K}(\omega)]$ is constructed directly using the expression of $\mathbb{a}(\mathbf{x},\omega)$ defined by Eq. (23) without computing the Hilbert transform of reduced matrix $[\mathcal{D}(\omega)]$. The graphs of $\nu \mapsto \|\widehat{\mathbf{q}}'(2\pi\nu)\|$ and $\nu \mapsto \|\widehat{\mathbf{q}}(2\pi\nu)\|$ for

ν in B_ν are shown in Fig. 3. The effects of the frequency-dependent stiffness matrix on the response of the structure are clearly seen in the frequency band of analysis.

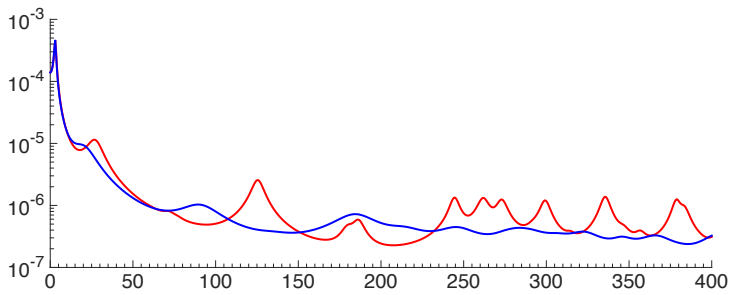

Figure 3 Graphs of $\nu \mapsto \|\widehat{\mathbf{q}}'(2\pi\nu)\|$ (blue line) and $\nu \mapsto \|\widehat{\mathbf{q}}(2\pi\nu)\|$ (red line). Horizontal axis: frequency ν in Hz.

Fig. 4 displays the graph of the relative error function

$$\omega \mapsto \mathrm{e}_r(\omega) = \frac{\|[\mathcal{K}^{\,\mathrm{ref}}(\omega)] - [\widetilde{\mathcal{K}}(\omega)]\|_F}{\|[\mathcal{K}^{\,\mathrm{ref}}(\omega)]\|_F} ,$$

in which $\|.\|_F$ denotes the Frobenius norm, where $[\mathcal{K}^{\,\mathrm{ref}}(\omega)]$ is the generalized stiffness matrix that is directly computed using the analytical expression of $\mathbb{o}(\mathbf{x}, \omega)$ defined by Eq. (23) (and called the reference), and where $[\widetilde{\mathcal{K}}(\omega)] = [\mathcal{K}_0] + [\mathcal{K}(\omega)]$ for which $[\mathcal{K}(\omega)]$ is computed using Eq. (37) with the numerical scheme presented in Section 4 for which $u_g = 100$, $N_u = 10,000$ and $N_q = 2$. A convergence analysis has been performed with respect to N_u and N_q yielding those values. It can be seen that the relative error is less than 10^{-5} in the frequency band B_ν of analysis and consequently, the computation of the Hilbert transform is very accurate. Figures 4 confirms that convergence is effectively reached. Fig. 5 displays the two graphs of the function $\omega \mapsto \|\widehat{\mathbf{q}}(\omega)\|$ that correspond (1) to the reference obtained by using $[\mathcal{K}^{\,\mathrm{ref}}(\omega)]$ and (2) to the use of $[\mathcal{K}(\omega)]$ that is computed with Eq. (37). It can be seen that there are almost no differences between the two graphs, and consequently, a validation of the method proposed is obtained.

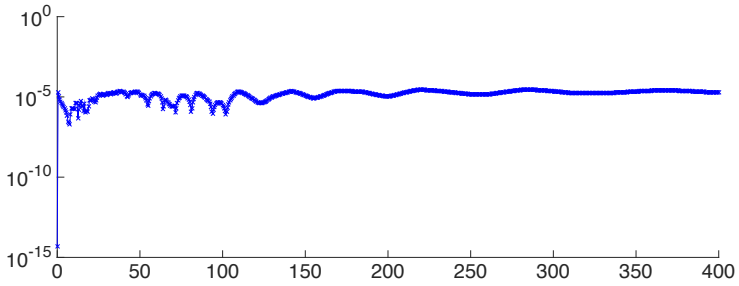

Figure 4 Graph of the relative error function $\nu \mapsto \mathrm{e}_r(2\pi\nu)$. Horizontal axis: frequency ν in Hz.

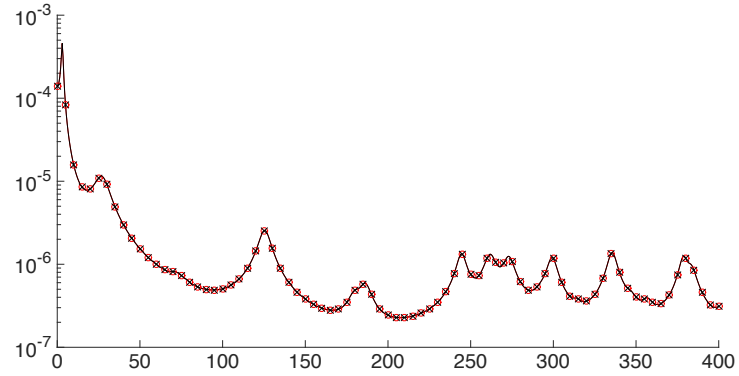

Figure 5 Graphs of $\nu \mapsto \|\widehat{\mathbf{q}}(2\pi\nu)\|$ corresponding to the reference (black crossed line) and by using the Hilbert transform of $[\mathcal{D}(\omega)]$ (red circles). Horizontal axis: frequency ν in Hz.

5.1.3. Uncertainty quantification

The Monte Carlo numerical method is used to solve the stochastic problem defined by Eqs. (39) and (40). The convergence analysis is carried out in analyzing the function $N_s \mapsto \mathrm{conv}(N_s)$ defined by

$$\mathrm{conv}(N_s) = \frac{1}{N_s} \sum_{k=1}^{N_s} \int_B \left\| \widehat{\mathbf{Q}}(\theta_k, \omega) \right\|^2 d\omega \,, \tag{85}$$

in which $\theta_1, \ldots, \theta_{N_s}$ correspond to N_s independent realizations. Fig. 6 displays the graph of $N_s \mapsto \mathrm{conv}(N_s)$. It can be seen that a reasonable mean-square convergence is reached for $N_s = 640$.

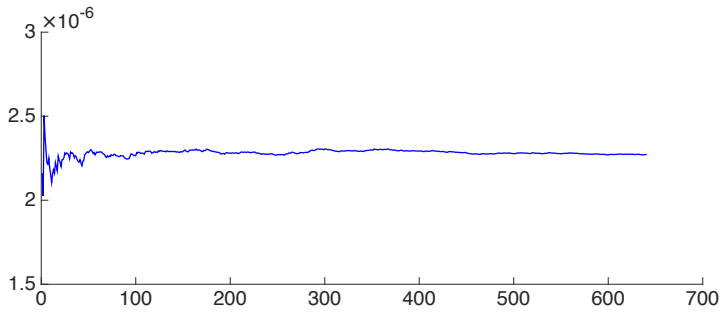

Figure 6 Graph of $N_s \mapsto \mathrm{conv}(N_s)$. Horizontal axis: number N_s of independent realizations.

Hereinafter, the two random models with almost-sure causality (see Eqs. (39) and (40)) and with the causality in mean (see Eqs. (47) and (48)) are compared. It is assumed that $[\mathbf{M}]$ remains deterministic ($\delta_M = 0$), and that $\delta_K = 0.15$ and $\delta_D = 0.7$. Let $\widehat{U}_k^{(N)}(\omega) = \{\widehat{\mathbb{U}}^{(N)}(\omega)\}_k$ be the k-th component of $\widehat{\mathbb{U}}^{(N)}(\omega) = [\Phi_N]\,\widehat{\mathbf{Q}}(\omega)$. Let $\widehat{u}_k^{(N)}(\omega) = \{\widehat{\mathbb{u}}^{(N)}(\omega)\}_k$ be the k-th component of the response calculated with computational model. The numbering of degrees of freedom is such that, for $k = 1, 2, 3$, $\widehat{U}_k^{(N)}(\omega)$ is related to the degree of freedom in direction $\mathbf{e}_k$ of the node located, respectively, at (0.5067 m, 0.1630 m, 0.1 m) (see Fig. 1), at (0.2 m, 0.1174 m, 0 m) (see Fig. 3), and at (1 m, 0.1696 m, 0.1 m) (see Fig. 1). For $k = 1$ and $k = 2$, the confidence region of the stochastic response $\omega \mapsto |\widehat{U}_k^{(N)}(\omega)|$ with a probability level $p_c = 0.95$, its statistical mean value, and the deterministic response $\omega \mapsto |\widehat{u}_k^{(N)}(\omega)|$, are displayed, for the random model with almost-sure causality, in Fig. 7 (for $k = 1$) and in Fig. 9 (for $k = 2$), and are displayed, for the random model with causality in mean, in Fig. 8 (for $k = 1$) and in Fig. 10 (for $k = 2$).

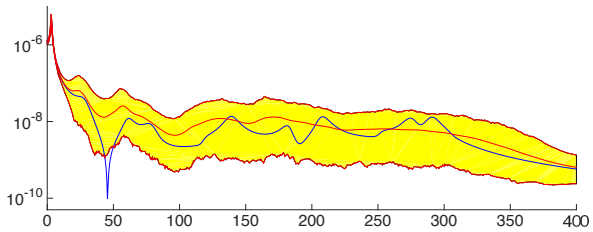

Figure 7 Graph of $\nu \mapsto |\widehat{U}_1^{(N)}(2\pi\nu)|$ for the probabilistic model with almost-sure causality: 95% confidence region (yellow region) and mean value (red line). Graph of $\nu \mapsto |\widehat{u}_1(2\pi\nu)|$ (blue line). Horizontal axis: frequency ν in Hz.

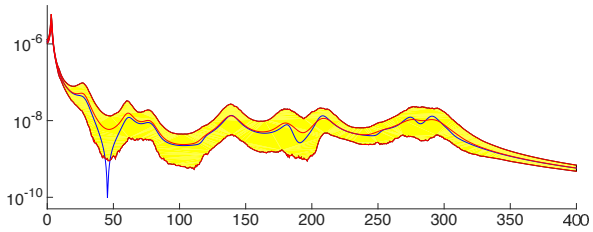

Figure 8 Graph of $\nu \mapsto |\widehat{U}_1^{(N)}(2\pi\nu)|$ for the probabilistic model with causality in mean: 95% confidence region (yellow region) and mean value (red line). Graph of $\nu \mapsto |\widehat{u}_1(2\pi\nu)|$ (blue line). Horizontal axis: frequency ν in Hz.

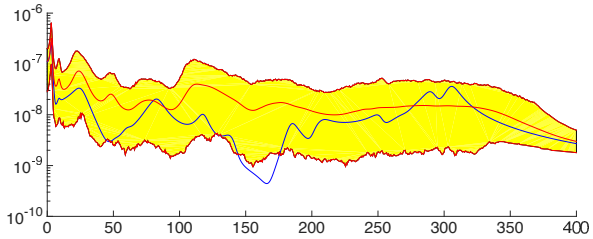

Figure 9 Graph of $\nu \mapsto |\widehat{U}_2^{(N)}(2\pi\nu)|$ for the probabilistic model with almost-sure causality: 95% confidence region (yellow region) and mean value (red line). Graph of $\nu \mapsto |\widehat{u}_2(2\pi\nu)|$ (blue line). Horizontal axis: frequency ν in Hz.

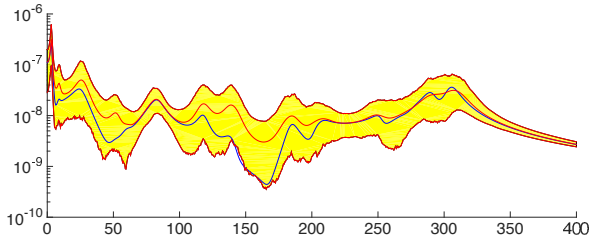

Figure 10 Graph of $\nu \mapsto |\widehat{U}_2^{(N)}(2\pi\nu)|$ for the probabilistic model with causality in mean: 95% confidence region (yellow region) and mean value (red line). Graph of $\nu \mapsto |\widehat{u}_2(2\pi\nu)|$ (blue line). Horizontal axis: frequency ν in Hz.

In Figs. 7 to 10, it can be seen that the confidence region is not the same for the probabilistic model with almost-sure causality and for the probabilistic model with causality in mean. The mean values are also different. It is important to note that in some cases, it can be seen that the values given by the computational model are outside of the 95% confidence interval for some frequencies, revealing that the computational model is not robust with respect to uncertainties for these frequencies.

Let $u \mapsto p_{|\widehat{U}_3^{(N)}|}(u;\omega)$ be the probability density function of $|\widehat{U}_3^{(N)}(\omega)|$. Figs. 11, 12, and 13 display the graphs of $u \mapsto p_{|\widehat{U}_3|}(u;2\pi\nu)$ at frequencies $\nu = 2$ Hz, $\nu = 200$ Hz, and $\nu = 400$ Hz, for the two probabilistic models with almost-sure causality (red line) and with causality in mean (blue line). Figs. 11 to 13 show that the probabilistic model with causality in mean does not give a good prediction (except for the low frequency 2 Hz that corresponds to a quasistatic response because the fundamental eigenfrequency is about 3 Hz).

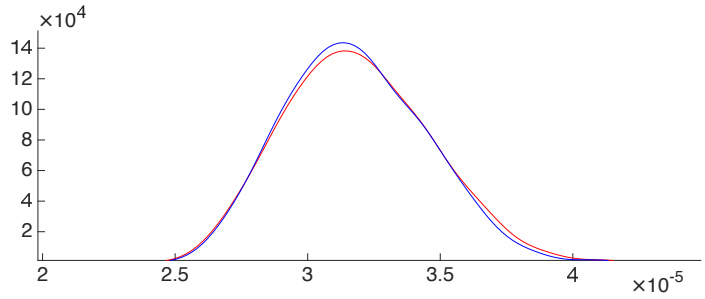

Figure 11 Graph of $u \mapsto p_{|\widehat{U}_3|}(u;2\pi\nu)$ at frequency $\nu = 2$ Hz. Probabilistic model with almost-sure causality (red line) and probabilistic model with causality in mean (blue line).

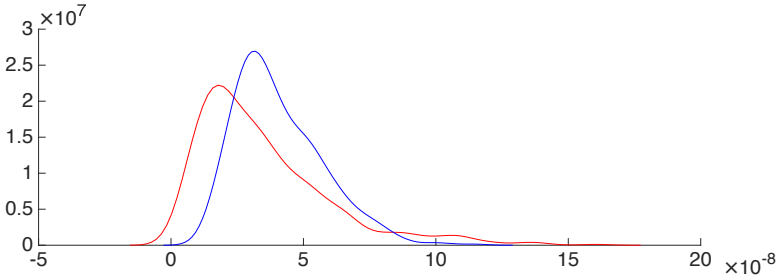

Figure 12 Graph of $u \mapsto p_{|\widehat{U}_3|}(u;2\pi\nu)$ at frequency $\nu = 200$ Hz. Probabilistic model with almost-sure causality (red line) and probabilistic model with causality in mean (blue line).

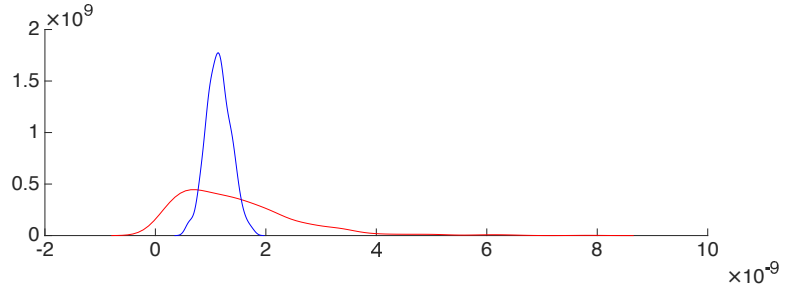

Figure 13 Graph of $u \mapsto p_{|\widehat{U}_3|}(u; 2\pi\nu)$ at frequency $\nu = 400$ Hz. Probabilistic model with almost-sure causality (red line) and probabilistic model with causality in mean (blue line).

Let $\delta_{[\widetilde{\mathbf{K}}]}(\omega)$ be the dispersion coefficient of the random matrix $[\widetilde{\mathbf{K}}(\omega)] = [\mathbf{K}_0] + [\mathbf{K}(\omega)]$, which is defined by

$$\delta_{[\widetilde{\mathbf{K}}]}(\omega) = \frac{E\{\left\| [\widetilde{\mathbf{K}}(\omega)] - E\{[\widetilde{\mathbf{K}}(\omega)]\} \right\|_F^2\}^{\frac{1}{2}}}{\left\| E\{[\widetilde{\mathbf{K}}(\omega)]\} \right\|_F} .$$

Fig. 14 displays the graph of $\omega \mapsto \delta_{[\widetilde{\mathbf{K}}]}(\omega)$ for the two probabilistic models, the one with almost-sure causality (red line) and the other one with causality in mean (blue line). It can be seen that, for the probabilistic model with causality in mean, $\omega \mapsto \delta_{[\widetilde{\mathbf{K}}]}(\omega)$ is approximatively constant in the frequency band of analysis, while for the probabilistic model with almost-sure causality, function $\omega \mapsto \delta_{[\widetilde{\mathbf{K}}]}(\omega)$ strongly increases in the frequency band of analysis and becomes constant with a multiplicative factor that is about 3. Such a result is consistent with the results presented in Figs. 7 to 13.

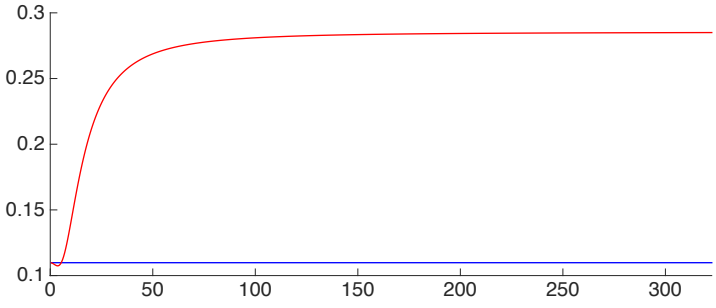

Figure 14 Graph of $\nu \mapsto \delta_{[\widetilde{\mathbf{K}}]}(2\pi\nu)$. Probabilistic model with almost-sure causality (red line) and probabilistic model with causality in mean (blue line). Horizontal axis: frequency ν in Hz.

6. Conclusion

In the framework of the nonparametric probabilistic approach of uncertainties, a new stochastic modeling has been proposed for taking into account uncertainties in the computational models of linear viscoelastic dynamical structures. This method is based on the construction of a compatibility equation that allows for satisfying the causality principle for the stochastic dynamical system in order to obtain compatible realizations of the random stiffness matrix and the random damping matrix at each frequency point of analysis. The numerical developments that are necessary for implementing the compatibility equation in the frequency domain has been detailed. The Cauchy principal-value integrals over a half-infinite interval are computed using a Gaussian quadrature for a certain class of functions, and an efficient interpolation technique has been introduced for computing a function with values in the positive-definite matrices, for a large number of sampling frequency points. The theory and the developments presented have been used for analyzing the propagation of uncertainties in a computational model of a composite viscoelastic structure. The results obtained show that it is very important to construct a probabilistic model which satisfies the causality principle. The theory presented has been done in the frequency domain and is independent of the choice of the reduced-order basis that is chosen for constructing the reduced-order model (any basis of the admissible vector space of the solution can be used). The method proposed could be used for a linear dynamical system made up of a linear viscoelastic structure that exhibits one or several rotating parts with a constant rotation speed. The reduced-order basis must be selected as explained in the literature and the stochastic model would be applied to each sub-domain described in the rotating frame. Concerning the capability of the model proposed to be applied to a linear viscoelastic structure with some local nonlinearities (such as stops), all the developments presented could be reused by using a Fourier transform to go from the time domain to the frequency domain, and then to come back in the time domain with an inverse Fourier transform.

References

[1] R.Ghanem, P.D.Spanos, Stochastic Finite Elements : A Spectral Approach, Springer-Verlag, NewYork, 1991 (Revised edition, Dover Publications, New York, 2003).

[2] C. Soize, A nonparametric model of random uncertainties for reduced matrix models in structural dynamics, Probabilistic Engineering Mechanics 15(3) (2000) 277-294.

[3] R. Mace, W. Worden, G. Manson, Uncertainty in structural dynamics, J. Sound Vib. 288(3) (2005) 431-790.

[4] G.I.Schueller (Ed.), Computational methods in stochastic mechanics and reliability analysis, Comput. Methods Appl. Mech. Engrg. 194(12-16) (2005) 1251-1795.

[5] C. Soize, Stochastic Models of Uncertainties in Computational Mechanics, American Society of Civil Engineers (ASCE), Reston, 2012.

[6] C. Soize, I.E. Poloskov, Time-domain formulation in computational dynamics for linear viscoelastic media with model uncertainties and stochastic excitation, Computers and Mathematics with Applications 64(11) (2012) 3594-3612.

[7] R. Ohayon, C. Soize, Advanced Computational Vibroacoustics, Cambridge University Press, New York, 2014.

[8] C. Soize, Stochastic modeling of uncertainties in computational structural dynamics - Recent theoretical advances, J. Sound Vib. 332(10) (2013) 2379-2395.

[9] C. Desceliers, C. Soize, S. Cambier, Non-parametric-parametric model for random uncertainties in non-linear structural dynamics: Application to earthquake engineering, Earthquake Engineering & Structural Dynamics 33(3) (2004) 315-327.

[10] M. Arnst, D. Clouteau, H. Chebli, R. Othman, G. Degrande, A non-parametric probabilistic model for ground-borne vibrations in buildings, Probabilistic Engineering Mechanics 21 (2006) 1834.

[11] E. Capiez-Lernout, M. Pellissitti, H. Pradlwarter, G.I. Schueller, C. Soize, Data and model uncertainties in complex aerospace engineering systems, J. Sound Vib. 295 (3-5) (2006) 923-938.

[12] C. Chen, D. Duhamel, C. Soize, Probabilistic approach for model and data uncertainties and its experimental identification in structural dynamics: Case of composite sandwich panels, J. Sound Vib. 294(1-2) (2006) 64-81.

[13] J.-F. Durand, C. Soize, L. Gagliardini, Structural-acoustic modeling of automotive vehicles in presence of uncertainties and experimental identification and validation, Journal of the Acoustical Society of America 124(3) (2008) 1513-1525.

[14] M.P. Mignolet, C. Soize, Stochastic reduced order models for uncertain nonlinear dynamical systems, Comput. Methods Appl. Mech. Engrg. 197(45-48) (2008) 3951-3963.

[15] C. Desceliers, G. Bonnet, S. Hamza, P. Delmotte, Mixed nonparametric-parametric probabilistic model for earthquake reliability of an inelastic reinforced concrete frame structure, Bulletin of Earthquake Engineering 8(4) 2010 921-935.

[16] A. Batou, C. Soize, M. Corus, Experimental identification of an uncertain computational dynamical model representing a family of structures, Computer and Structures 89(13-14) (2011) 1440-1448.

[17] E. Capiez-Lernout, C. Soize, M.-P. Mignolet, Computational stochastic statics of an uncertain curved structure with geometrical nonlinearity in three dimensional elasticity, Computational Mechanics 49(1) (2012) 87-97.

[18] R. Murthy, X.Q.Wang, R. Perez, M.P. Mignolet, L.A. Richter, Uncertainty-based experimental validation of nonlinear reduced order models, J. Sound Vib. 331 (2012) 1097-1114.

[19] M.P. Mignolet, C. Soize, J. Avalos, Nonparametric stochastic modeling of structures with uncertain boundary conditions / coupling between substructures, AIAA Journal 51(6) (2013) 1296-1308.

[20] A. Batou, C. Soize, S. Audebert, Model identification in computational stochastic dynamics using experimental modal data, Mechanical Systems and Signal Processing 50-51 (2014) 307-322.

[21] E. Capiez-Lernout, C. Soize, M.P. Mignolet, Post-buckling nonlinear static and dynamical analyses of uncertain cylindrical shells and experimental validation, Comput. Methods Appl. Mech. Engrg. 271(1) (2014) 210-230.

[22] C. Truesdell, Encyclopedia of Physics, Vol. VIa/3, Mechanics of Solids III, Springer-Verlag, Berlin, 1973.

[23] R.M. Christensen, Theory of Viscoelasticity (Second Edition), Academic Press, 1982.

[24] C. Soize, R. Ohayon, Structural Acoustics and Vibration, Academic Press, 1998.

[25] H.A. Kramers, La diffusion de la lumiere par les atomes, Atti Cong. Intern. Fisica, (Transactions of Volta Centenary Congress) Como 2 (1927) 545-557.

[26] R.D. Kronig, On the theory of dispersion of X-rays, J. Opt. Soc. Amer. 12(6) (1926) 547-557.

[27] A. Papoulis, Signal Analysis, McGraw-Hill, New York, 1977.

[28] R.Y. Rubinstein, Simulations and the Monte Carlo Methods, John Wiley and Sons, New York, 1981.

[29] M.H. Kalos, P.A. Whitlock, Monte Carlo Methods, Volume 1: Basics, John Wiley and Sons, Chichester, 1986.

[30] W. Gautschi, Gauss-type quadrature rules for rational functions, Internat. Ser. Numer. Math. 112 (1993) 111-130.

[31] W. Gautschi, The use of rational functions in numerical quadrature, Journal of Computational and Applied Mathematics 133(1-2) (2002) 111-126.

[32] W. Gautschi, Orthogonal polynomials and special Functions, pp. 1-77, in Orthogonal Polynomials, Quadrature, and Approximation: Computational Methods and Software (in Matlab), Springer, Berlin, 2006.

[33] C. Soize, C. Desceliers, Computational aspects for constructing realizations of polynomial chaos in high dimension, SIAM Journal on Scientific Computing 32(5) (2010) 2820-2831.

[34] G. Perrin, C. Soize, D. Duhamel, C. Funfschilling, Identification of polynomial chaos representations in high dimension from a set of realizations, Journal on Scientific Computing 34(6) (2012) A2917-A2945.

[35] K.J. Bathe. *Finite Element Procedures*, Prentice Hall, 1996.

[36] O.C. Zienkiewicz, R.L. Taylor. *The Finite Element Method Set (Sixth Edition)*, Butterworth-Heinemann, 2005.

[37] H.J. Pradlwarter, G.I. Schueller, On advanced Monte Carlo simulation procedures in stochastic structural dynamics, Internat. J. Non-Linear Mech. 32(4) (1997) 735-744.